Towards advanced aqueous zinc battery by exploiting synergistic effects between crystalline phosphide and amorphous phosphate

Shunshun Zhao[1§], Guangmeng Qu[2§], Chenggang Wang[2], Yujin Zhang[1], Chuanlin Li[2], Xiaojuan Li[2], Jie Sun[1]*, Jiancai Leng[1]*, Xijin Xu[2]*

[1]School of Electronic and Information Engineering (Department of Physics), Qilu University of Technology (Shandong Academy of Sciences), 250353 Jinan, Shandong, P. R. China;

[2]School of Physics and Technology, University of Jinan, 336 West Road of Nan Xinzhuang, Jinan 250022, Shandong, P. R. China;

E-mails: sps_xuxj@ujn.edu.cn; phys_xu@hotmail.com

[§]The authors contribute equally to the work.

SUPPLEMENTARY INFORMATION

Experimental section

Preparation of NiCo-BHs precursor on Ni foam (NF): The NF (2×3cm, 500μm) is alternately cleaned with acetone, hydrochloric acid, ethanol and deionized water for 30 minutes to remove surface inclusions, and then dried at 60 °C in the vacuum drying chamber. 2 mmol cobalt chloride hexahydrate ($CoCl_2·6H_2O$), 1 mmol nickel chloride hexahydrate ($NiCl_2·6H_2O$), 6 mmol urea ($CO(NH_2)_2$) and 1 mmol hexadecyl trimethyl ammonium bromide (CTAB) are dissolved into 35 mL deionized water and stirred for 20 minute to form a pink clear solution. Afterwards the above solution and a pretreated NF were transferred into a 50 mL Teflon-lined stainless steel autoclave.

The hydrothermal process needs to be maintained at 100 ℃ for 6 h，and then cooled to room temperature naturally. The NF was thoroughly washed with deionized water and ethanol and dried at 60 ℃ for 12 h in an oven to get NiCo-BHs/NF precursor.

Preparation of NiCoP: The as-prepared NiCo-BHs/NF precursor were annealed in atmosphere at 300 °C for 0.5 h the heating rate of 2 °C min^{-1}. Then in a tubular furnace, using sodium hypophosphite ($NaH_2PO_2·H_2O$, 100 mg) as the source of phosphorus, NiCoP/NF can be obtained at 350 ℃ (heating rate of 2 °C min^{-1}) for 1 h under gently flowing Ar (flowing rate of 60 mL min^{-1}). The areal mass loadings of the NiCoP were approximately 1.2~1.3 mg cm^{-2}.

Preparation of C-NiCoP@A-$NiCoPO_4$: Firstly, the electrolyte is prepared. $Co(NO_3)_2·6H_2O$ (1 mmol), $Ni(NO_3)_2·6H_2O$ (1 mmol), and $NaH_2PO_2·H_2O$ (1 mmol) were dissolved in 100 mL of the mixture of ethanol and deionized water (v/v = 1:1) in a 200 mL beaker. The electrodynamic deposition was carried out in a three-electrode cell using NiCoP/NF (2 × 2 cm^2) as the working electrode, Pt foil as counter electrode, and Ag/AgCl as reference electrode by cyclic voltammetry at a scan rate of 5 mV s^{-1} for 6 cycles within a voltage range of −1.2 to 0.2 V. The electrodeposited material was placed in a drying oven at 60 ℃ for 6 hours to obtain C-NiCoP@A-$NiCoPO_4$. The areal mass loadings of the C-NiCoP@A-$NiCoPO_4$ samples were about 1.5 mg cm^{-2}.

Preparation of the PAM hydrogel electrolyte: Firstly, 6 g acrylamide monomer was added to 20 mL electrolyte (3M KOH+0.03M zinc acetate ($Zn(Ac)_2$) and stirred for 1 h. Then, 75 mg ammonium persulphate (APS) functioning as the initiator and 4 mg of N,N′-methylenebis(acrylamide) (MBAA) as crosslinker were added into the

above solution and stirred for 2 h at 20 °C. After the solution was bubbled by N_2 for 10 mins and degassed in a vacuum chamber. Lastly, the as-obtained solution was injected into a glass mold and maintained at 70 °C for 1 h. When cooled naturally to room temperature, the flexible hydrogel electrolyte was obtained.

Computational details

All computational simulations are performed based on density functional theory (DFT) with the projector-augmented wave (PAW) method.[1] The Vienna ab initio simulation package (VASP) is used for geometry optimizations and electronic structure calculations. The generalized gradient approximation of Perdew-Burke-Ernzerhof (GGA-PBE)[2] is introduced into the exchange-correlation functional to improve the calculation accuracy. The plane-wave cutoff energy is 450 eV and the Brillouin zone is sampled in k-space using a Monkhorst-Pack scheme of 2×2×2. All structures were fully relaxed to the ground state and spin-polarization was considered in all calculations.[3] The convergence criteria of all computational simulations were set as 10^{-5} eV in energy and 0.02 eV/Å in force. To correct the incomplete cancelation of the self-interaction of the GGA, the Hubbard parameters (GGA+U) were used.[4] Effective U-values of 5.0 eV and 5.6 eV for Co and Ni ion were used, respectively.[5] Meanwhile, in order to better simulate amorphous $NiCoPO_4$, disordered phosphate ions were coated on the surface of NiCoP. The above parameters are used to optimize the structure model to minimize its energy. The obtained relaxation model is used as the basis for subsequent calculation.

Materials characterization

The micro-nano morphology of prepared electrode materials was observed by a field emission scanning electron microscope (SEM, Hitachi S4800). The composition of the material was determined by X-ray diffraction (XRD, D8-Advance Bruker), and more detailed nanostructures measurement were performed by transmission electron microscope (TEM, talos F200X) equipped with energy dispersive X-ray spectrometer (EDS). The X-ray photoelectron spectroscopy (XPS, Thermo ESCALAB250Xi) was applied to characterize the chemical valence states and chemical compositions. Valence states and chemical compositions of prepared materials were characterized by X-ray photoelectron spectroscopy (XPS, Thermo Scientific). The N_2 absorbing/desorbing isotherms were measured to analyze specific surface areas and pore distribution by Brunauer-Emmett-Teller (BET) and Barrett-Joyner-Halenda (BJH) methods.

Electrochemical measurements

The electrochemical properties were studied by a typical three-electrode system with a Pt foil counter electrode, a Hg/HgO reference electrode and 3M KOH electrolyte. The cyclic voltammetry (CV) curve and galvanostatic charge-discharge (GCD) curve were tested on the electrochemical workstation (CHI 660E). The electrochemical impedance spectroscopy (EIS) measurements was measured using the Autolab PGSTAT 302N electrochemical workstation (Metrohm AG, Herisau, Switzerland) at frequency of 0.01 Hz~100 KHz.

The aqueous pouch cells were assembled by applying synthesized C-NiCoP@A-$NiCoPO_4$ as cathode, a Zn foil (2×3, 100 μm) as anode, 3M

KOH+0.03M zinc acetate ($Zn(Ac)_2$), and a nonwoven diaphragm as separator. The GITT and uninterrupted charge/discharge measurement of assembled cell was performed in a LAND battery measurement tester.

According to the results of the as-obtained GCD curve profiles, the following formula[6] is employed to calculate the capacity of the synthesized prepared material and assembled cell：

$$C_m = \frac{\int_0^t Idt}{m} \tag{S1}$$

in which Cm (mAh g^{-1}) refers to the capacity, I (mA) and t (h) are current and time over the discharge process, m is mass loading (g) of active material loading on the Ni foams.

GITT tests were performed with a current density of 20 mA g^{-1} for 10 min repeating discharge current pulse and relaxation. The diffusion coefficient is calculated based on following equation[7]:

$$D^{GITT} = \frac{4}{\pi\tau}(\frac{mV_M}{MS})^2(\frac{\Delta E_s}{\Delta E_t})^2 \tag{S2}$$

in which τ and ΔEt are duration of the current pulse (10 min) and potential alteration caused by this duration, m, V, M and S refer to the mass loading, molar volume, molecular weight and contact area with electrolyte of active materials, respectively, and ΔEs represents the difference in open circuit voltage.

The flexible battery was assembled using synthesized C-NiCoP@A-$NiCoPO_4$ as a positive electrode, a zinc sheet (1×3, 100 μm) as a negative electrode and the PAM

hydrogel electrolyte as a diaphragm. we characterized the performance of flexible battery subjected to different bending angles.

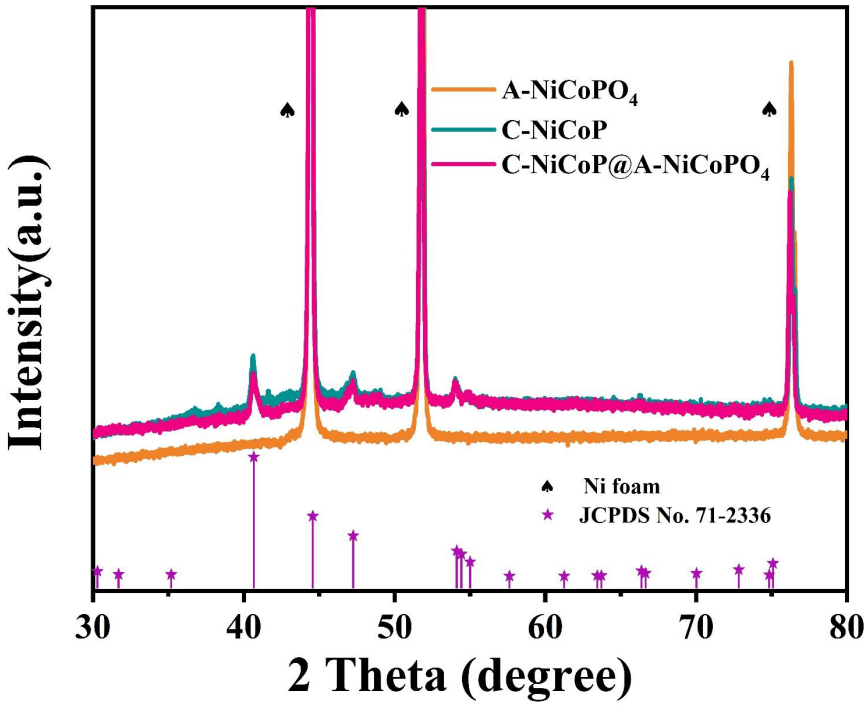

Fig. S1 XRD patterns of $NiCoPO_4$, C-NiCoP and C-NiCoP@A-$NiCoPO_4$.

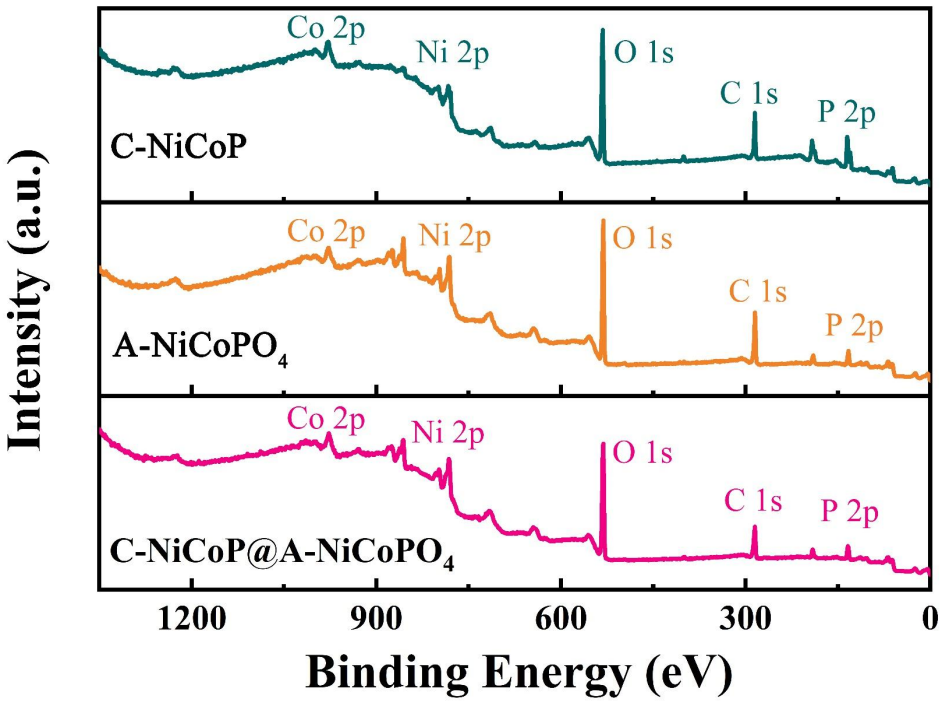

Fig. S2 XPS spectra of C-NiCoP, A-NiCoPO$_4$ and C-NiCoP@A-NiCoPO$_4$.

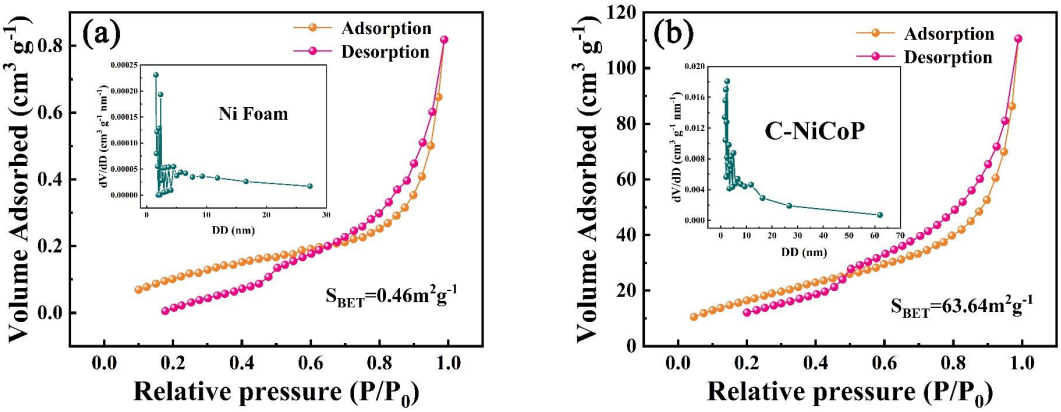

Fig. S3 N_2 adsorption-desorption isotherm and pore size distribution plots. (a) Ni Foam; (b) C-NiCoP.

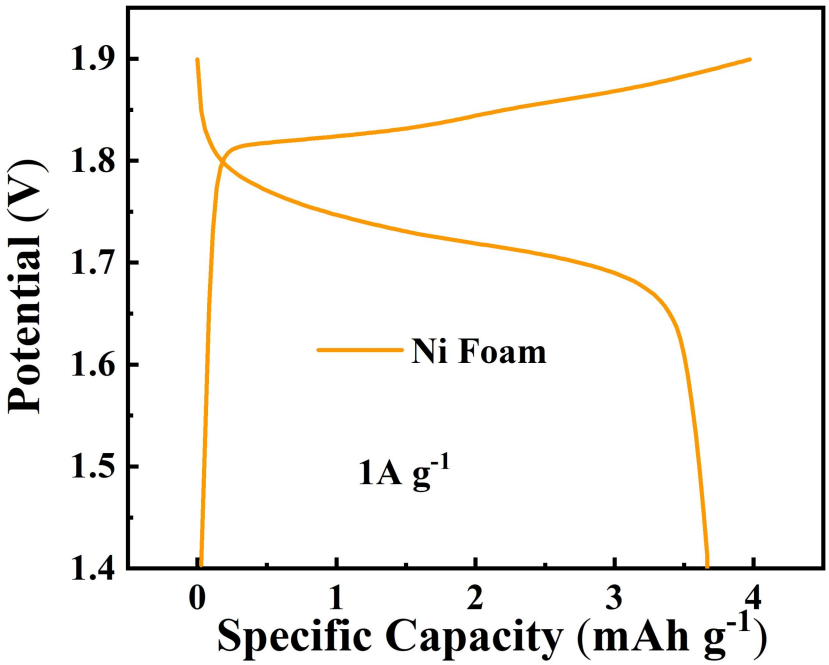

Fig. S4 GCD curves of pure NF at 1 A g^{-1}.

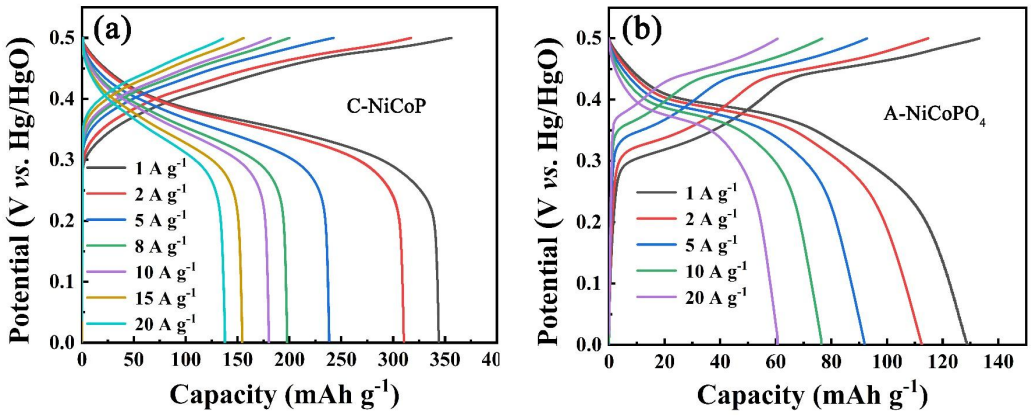

Fig. S5 GCD curves at varied current densities: (a) C-NiCoP; (b) A-$NiCoPO_4$.

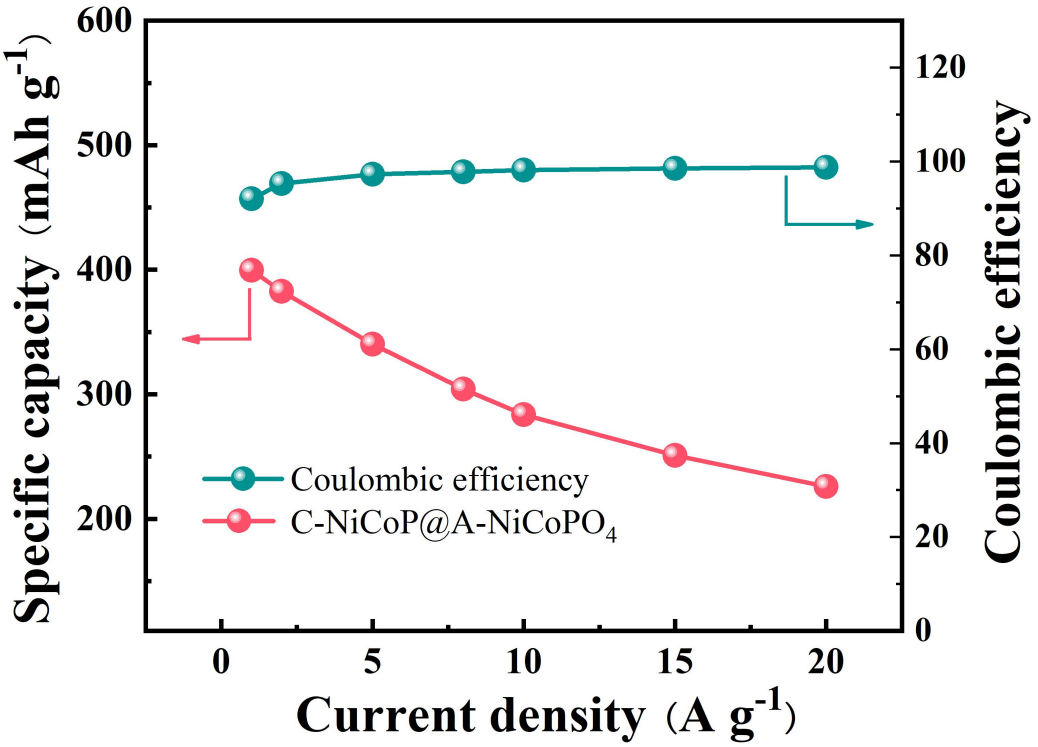

Fig. S6 Specific capacities and coulombic efficiencies of C-NiCoP@A-NiCoPO$_4$ at different current densities.

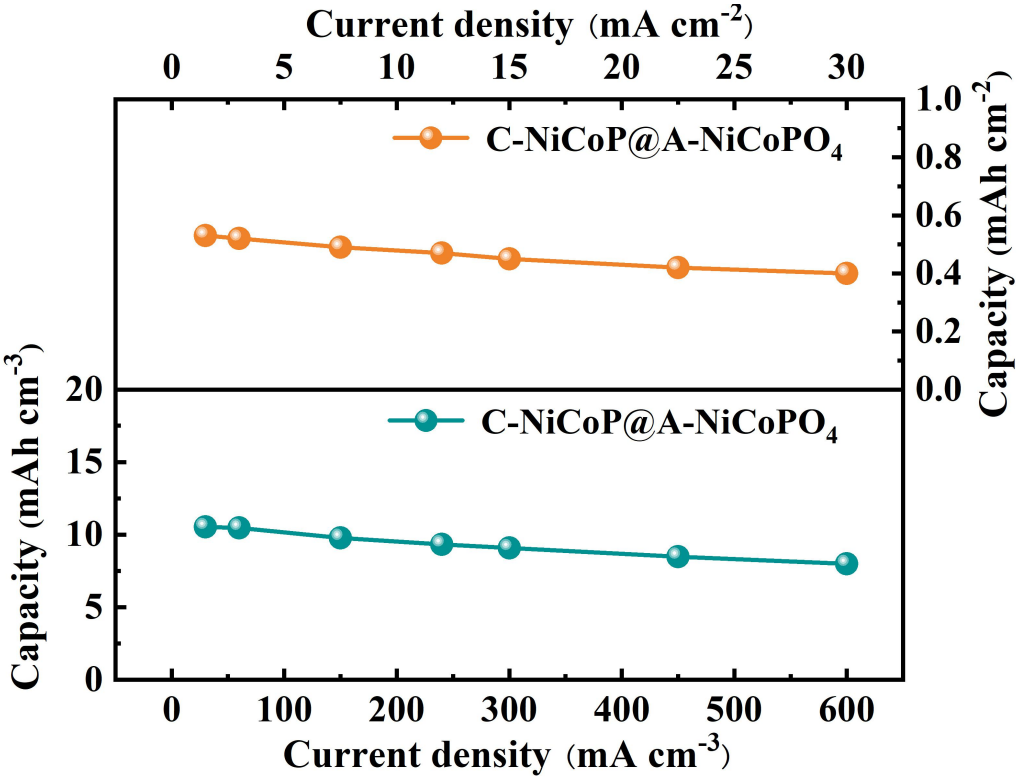

Fig. S7 The areal and volumetric capacities of C-NiCoP@A-$NiCoPO_4$ at different current densities.

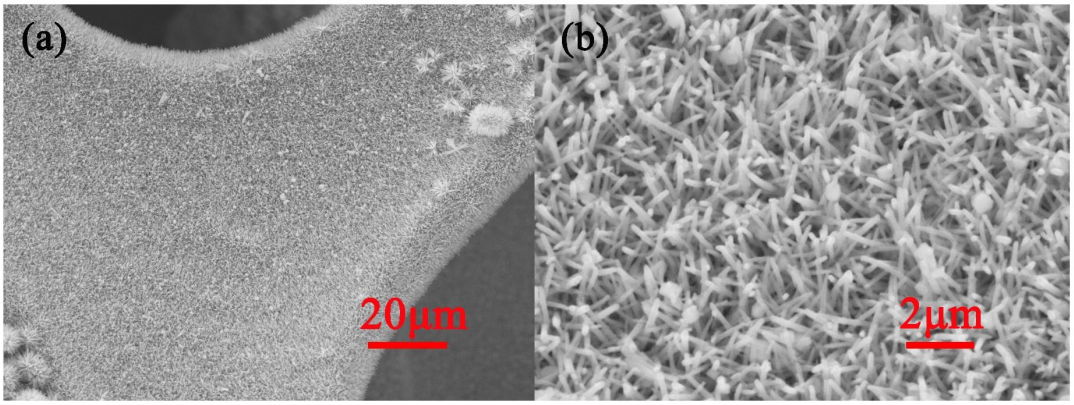

Fig. S8 SEM image of C-NiCoP@A-$NiCoPO_4$ after 10000 cycles at 10 A g^{-1}.

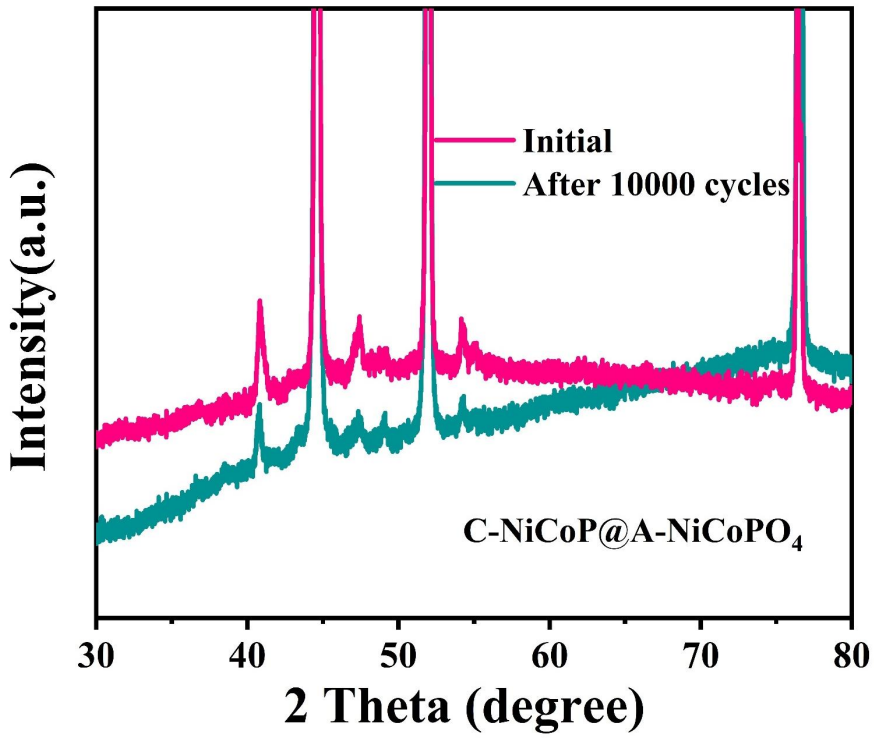

Fig. S9 XRD patterns of C-NiCoP@A-NiCoP after 10000 cycles.

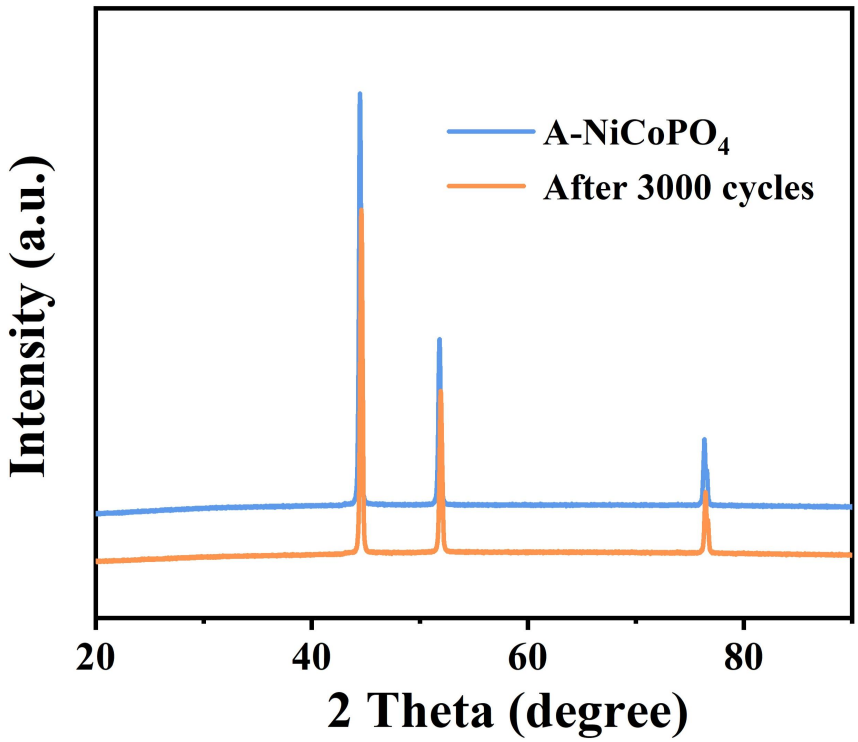

Fig. S10 XRD patterns of A-NiCoPO$_4$ after 3000 cycles.

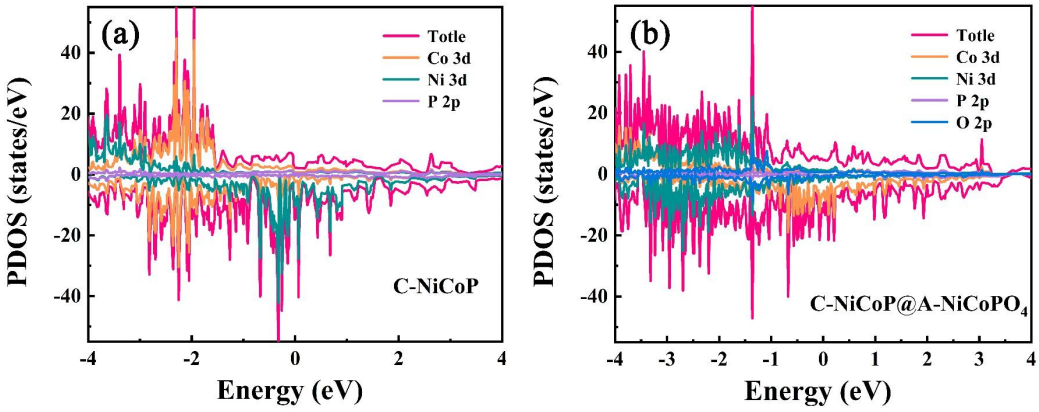

Fig. S11 PDOS of C-NiCoP (a) and C-NiCoP@A-NiCoPO$_4$ (b).

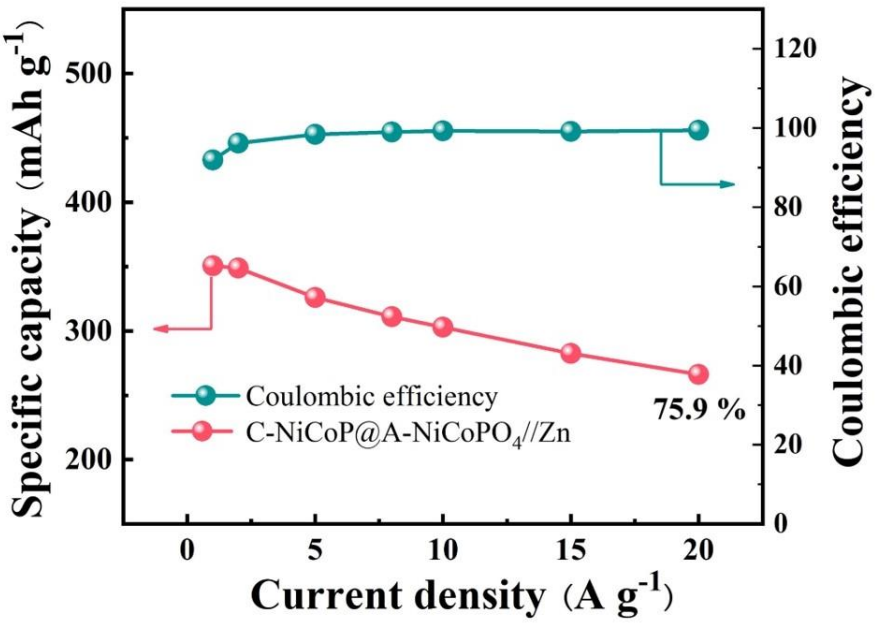

Fig. S12 Specific capacities and coulombic efficiencies of C-NiCoP@A-NiCoPO4//Zn at different current densities.

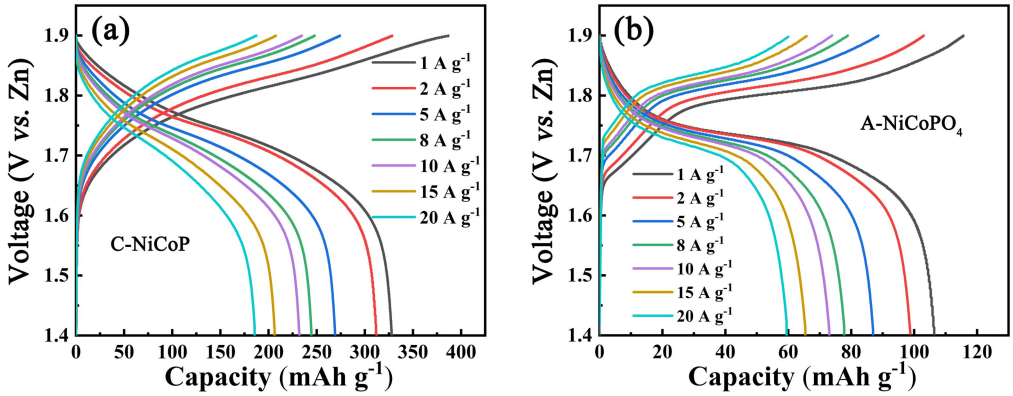

Fig. S13 GCD curves at varied current densities. (a) C-NiCoP//Zn; (b) A-NiCoPO4//Zn.

Table 1 A comparison of current C-NiCoP@A-$NiCoPO_4$ with previously reported of aqueous Zn batteries.

Electrode materials	Middle discharge voltage (V)	Specific capacity (mAh g^{-1})	Cycle stability	Ref.
C-NiCoP@A-$NiCoPO_4$	1.72	358.3	95.7%(7k)	Our work1
C-NiCoP@A-$NiCoPO_4$	1.71	348.5	87.3%(3k)	Our work2
MnO_2@CNT	1.2	290	75%(300)	8
$NiCo_2O_4$	1.68	230	63.26%(1k)	9
Co_3S_4	1.63	317	96.5%(5k)	10
NiMn-LDH	1.65	180	100%(1k)	11
$NiMoO_4$	1.72	165	85.9%(3k)	12
$Zn_3V_2O_7(OH)_2 \cdot 2H_2O$	0.85	240	68%(300)	13
Mn_2O_3	1.38	262	99%(120)	14
MnS	1.4	116	82.8%(1k)	15
h-VOW	0.85	250	85%(1.2k)	16
δ- MnO_2	1.2	278	98%(10k)	17

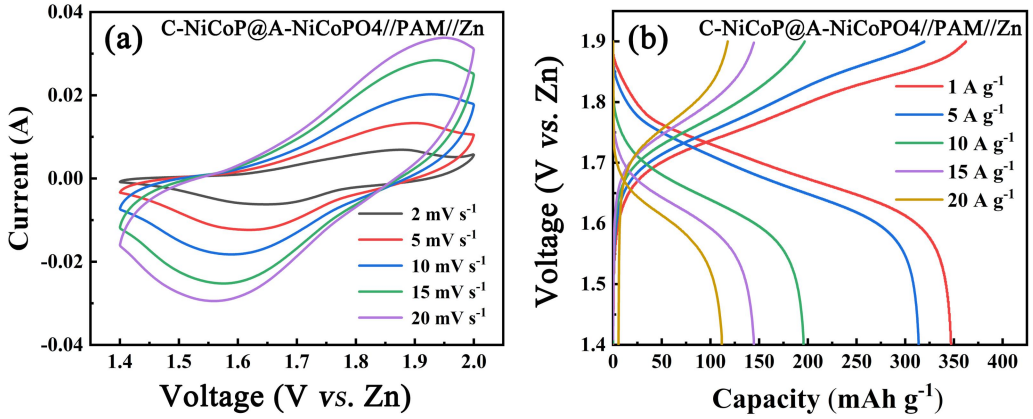

Fig. S14 (a) CV curves at varied current densities, (b) GCD curves at varied current densities of C-NiCoP@A-$NiCoPO_4$//PAM//Zn.

References:

1. G. Kresse and J. Hafner, *Physical Review B*, 1993, **47**, 558.

2. J. P. Perdew, K. Burke and M. J. P. r. l. Ernzerhof, *Phys. Rev. Lett,* 1996, **77**, 3865.

3. L.-Y. Gan, Q. Zhang, Y. Cheng and U. J. P. R. B. Schwingenschlögl, *Physical Review B*, 2013, **88**, 235310.

4. S. Dudarev, G. Botton, S. Savrasov, C. Humphreys and A. Sutton, *Physical Review B*, 1998, **57**, 1505.

5. C. E. Calderon, J. J. Plata, C. Toher, C. Oses, O. Levy, M. Fornari, A. Natan, M. J. Mehl, G. Hart and M. Nardelli, *Computational Materials Science*, 2015, **108**, 233-238.

6. K. A. Owusu, L. Qu, J. Li, Z. Wang, K. Zhao, C. Yang, K. M. Hercule, C. Lin, C. Shi and Q. J. Wei, *Chemical Communications*, 2017, **8**, 1-11.

7. W. Weppner and R. A. Huggins, *Journal of The Electrochemical Society,* 1977, **124**, 1569.

8. K. Wang, X. Zhang, J. Hang, X. Zhang, X. Sun, C. Li, W. Liu, Q. Li and Y. Ma, *Applied Materials & Interfaces*, 2018, **10,** 24573-24582.

9. W. Shang, W. Yu, P. Tan, B. Chen, H. Xu and M. J. Ni, *Journal of Power Sources*, 2019, **421,** 6-13.

10. S.W. Zhang, B.-S. Yin, Y.-Z. Luo, L. Shen, B.-S. Tang, Z. Kou, X. Liu, D.-M. Gu, Z.-B. Wang and H. J. Gong, *Nano Energy*, 2020, **68,** 104314.

11. S. Wang, X. Duan, T. Gao, Z. Wang, D. Zhou, K. Sun, Z. Shang, Y. Kuang, S. Tian and X. Li, *Journal of The Electrochemical Society*, 2020, **167,** 160550.

12. L. Zhou, S. Zeng, D. Zheng, Y. Zeng, F. Wang, W. Xu, J. Liu and X. Lu, *Chemical Engineering Journal*, 2020, **400,** 125832.

13. C. Xia, J. Guo, Y. Lei, H. Liang, C. Zhao and H. N. Alshareef, *Advanced Materials*, 2018, **30,** 1705580.

14. D. Feng, T. Gao, L. Zhang, B. Guo, S. Song, Z. Qiao and S. Dai, *Nano-Micro Letters*, 2020, **12,** 1-13.

15. X. Chen, W. Li, Y. Xu, Z. Zeng, H. Tian, M. Velayutham, W. Shi, W. Li, C. Wang and D. Reed, *Nano Energy*, 2020, **75,** 104869.

16. X. Li, L. Ma, Y. Zhao, Q. Yang, D. Wang, Z. Huang, G. Liang, F. Mo, Z. Liu and C. Zhi, *Angewandte Chemie International Edition*, 2019, **14,** 100361.

17. D. Wang, L. Wang, G. Liang, H. Li, Z. Liu, Z. Tang, J. Liang and C. Zhi, *ACS Nano*, 2019, **13,** 10643-10652.